ORIGINAL ARTICLE
BASIC SCIENCE

The mononuclear phagocyte system contributes to fibrosis in post-transplant obliterans bronchiolitis

Maria-Pia Di Campli[1,2,3], Abdulkader Azouz[1,2], Assiya Assabban[1,2], Jessika Scaillet[1,2], Marion Splittgerber[1,2], Alexandra Van Keymeulen[4], Frederick Libert[5], Myriam Remmelink[6], Alain Le Moine[1,2], Philippe Lemaitre[7] and Stanislas Goriely[1,2]

Affiliations: [1]Institute for Medical Immunology, Université Libre de Bruxelles, Gosselies, Belgium. [2]ULB Center for Research in Immunology (U-CRI), Université Libre de Bruxelles, Gosselies, Belgium. [3]Dept of Surgery, Erasme Hospital, Université Libre de Bruxelles, Brussels, Belgium. [4]Laboratory of Stem Cells and Cancer, Université Libre de Bruxelles, Brussels, Belgium. [5]BRIGHTcore ULB VUB and Institute of Interdisciplinary Research in Human and Molecular Biology (IRIBHM), Université Libre de Bruxelles, Brussels, Belgium. [6]Dept of Pathology, Erasme Hospital, Université Libre de Bruxelles, Brussels, Belgium. [7]Division of Thoracic Surgery, Lung Transplant Program, Columbia University Medical Center, New York, NY, USA.

Correspondence: Stanislas Goriely, Institute for Medical Immunology, 8 Rue Adrienne Bolland, B-6041 Charleroi-Gosselies, Belgium. E-mail: stgoriel@ulb.ac.be

@ERSpublications
Bronchiolitis obliterans syndrome remains a major cause of mortality after lung transplantation. The mononuclear phagocyte system actively contributes to fibrotic occlusion of rejected airways, thereby representing a promising novel therapeutic target. https://bit.ly/3hQh8UL

Cite this article as: Di Campli M-P, Azouz A, Assabban A, *et al*. The mononuclear phagocyte system contributes to fibrosis in post-transplant obliterans bronchiolitis. *Eur Respir J* 2021; 57: 2000344 [https://doi.org/10.1183/13993003.00344-2020].

ABSTRACT Bronchiolitis obliterans syndrome (BOS) is a fibrotic disease that is heavily responsible for the high mortality rates after lung transplantation. Myofibroblasts are primary effectors of this fibrotic process, but their origin is still debated. The purpose of this work was to identify the precursors of mesenchymal cells responsible for post-transplant airway fibro-obliteration.

Lineage-tracing tools were used to track or deplete potential sources of myofibroblasts in the heterotopic tracheal transplantation model. Allografts were analysed by histology, confocal microscopy, flow cytometry or single-cell transcriptomic analysis. BOS explants were evaluated by histology and confocal microscopy.

Myofibroblasts in the allografts were recipient-derived. When recipient mice were treated with tacrolimus, we observed rare epithelial-to-mesenchymal transition phenomena and an overall increase in donor-derived myofibroblasts (p=0.0467), but the proportion of these cells remained low (7%). Haematopoietic cells, and specifically the mononuclear phagocyte system, gave rise to the majority of myofibroblasts found in occluded airways. Ablation of $Cx3cR1^{+}$ cells decreased fibro-obliteration (p=0.0151) and myofibroblast accumulation (p=0.0020). Single-cell RNA sequencing revealed similarities between myeloid-derived cells from allografts and both murine and human samples of lung fibrosis. Finally, myofibroblasts expressing the macrophage marker CD68 were increased in BOS explants when compared to controls (14.4% *versus* 8.5%, p=0.0249).

Recipient-derived myeloid progenitors represent a clinically relevant source of mesenchymal cells infiltrating the airways after allogeneic transplantation. Therapies targeting the mononuclear phagocyte system could improve long-term outcomes after lung transplantation.

This article has an editorial commentary: https://doi.org/10.1183/13993003.04466-2020

This article has supplementary material available from erj.ersjournals.com

Data availability: Raw scRNA-seq data can be accessed on GEO (accession number GSE160760).

Received: 17 Feb 2020 | Accepted: 16 Sept 2020

Introduction

Lung transplantation is the only therapeutic option for some patients with end-stage respiratory diseases. Even though there has been an increase in terms of survival post-lung transplantation during the last decades, the proportion of patients developing bronchiolitis obliterans syndrome (BOS), a form of chronic lung allograft dysfunction, has remained unchanged [1]. BOS, with its histological counterpart obliterans bronchiolitis (OB), affects one out of two patients at 5 years post-transplant, and is heavily responsible for the limited long-term survival after lung transplantation [2]. Repetitive aggression against the respiratory epithelium causes its progressive destruction, leading to aberrant airway fibrosis and respiratory failure [3]. A general feature of fibrotic diseases is the progressive accumulation of myofibroblasts, defined as α-smooth muscle actin-positive (αSMA^+) fibroblasts that synthesise extracellular matrix components [4]. Their origin, however, remains highly controversial. They may arise from resident fibroblasts, pericytes, endothelial and epithelial cells or circulating precursors [5–8]. The identity of these bone marrow progenitors and their connection to other myeloid cells is elusive. Recent studies redefined the ontogeny of monocytes, macrophages and dendritic cells, which have been collectively termed the "mononuclear phagocyte system" (MPS) [9].

In the context of BOS, *ex vivo* studies concluded that myofibroblasts arise mainly from donor-derived progenitors [10, 11]. Accordingly, *in vivo* investigations, supported by *ex vivo* and *in vitro* findings [12, 13], have suggested the involvement of epithelial-to-mesenchymal transition (EMT) [14]. By contrast, another study concluded that, during allograft rejection, myofibroblasts are mostly recipient-derived [15].

We have used genetic fate mapping strategies [4] to show that the majority of myofibroblasts in rejected grafts after heterotopic tracheal transplantation (HTT) are recipient-derived, even under immunosuppression with tacrolimus. We have further demonstrated that most of these mesenchymal cells arise from myeloid precursors and that selective depletion of $Cx3cR1^+$ mononuclear phagocytes decreases the accumulation of myofibroblasts and lumen fibrosis in the allografts. Finally, we have identified myofibroblasts co-expressing the macrophage marker CD68 in patient samples. Collectively, these data support the involvement of myeloid-derived myofibroblasts in human BOS development after lung transplantation.

Methods

Mice

Detailed information concerning transgenic mouse strains and reference numbers can be found in the extended methods section of the supplementary material. Tamoxifen citrate-containing mouse chow was used to induce Cre recombinase activity. Some of the mice received an intraperitoneal injection of 1 $mg \cdot kg^{-1} \cdot day^{-1}$ of tacrolimus or vehicle only from transplantation until harvesting day. This study was approved by the Institutional Animal Care and Use Committee of the Biopark Université Libre de Bruxelles Charleroi (BUC), Charleroi, Belgium.

HTT model

HTT was performed by adapting the murine model developed by Hertz *et al.* [16] and has previously been used in our laboratory as described by Lemaître *et al.* [17].

Human samples

All human *ex vivo* samples were obtained by Erasme Hospital biobank (BE_BERA1; Biobanque Hôpital Erasme-Université Libre de Bruxelles (BERA); BE_NBWB1; Biothèque Wallonie Bruxelles; BBMRI-ERIC) with the approval of the ethics committee of Erasme Hospital, Université Libre de Bruxelles, Brussels. Samples were obtained from lung explants of patients undergoing a second transplant for BOS. Specimens showing healthy peripheral tissue from patients undergoing pulmonary resection for well-delimited carcinoid tumour were used as controls.

Statistical analysis

GraphPad Prism software v6.01 (GraphPad Software, La Jolla, CA, USA) was used to compare two data sets (Mann–Whitney nonparametric t-test) or more than two groups (Kruskal–Wallis test with Dunn's multiple comparisons test), and to establish correlations (Spearman's correlation test).

See the supplementary material for detailed information on experimental procedures.

Results

Myofibroblasts in post-transplant obliterative lesions are recipient-derived

Allogeneic HTT is a widely used experimental model of BOS because it recapitulates many of its histological features and leads to a progressive intraluminal fibrotic lesion named obliterative airway disease (OAD) [16, 17]. To discriminate between cells that were recipient- or donor-derived, we

transplanted tracheas from wild-type BALB/c mice into Ubi-GFP C57BL/6 mice, which express enhanced GFP under the direction of the human ubiquitin C promoter in all tissues (figure 1a). Histological analysis at day 28 post-transplantation showed a complete loss of the epithelium, with replacement by fibrotic tissue, in the allografts, whereas the syngeneic grafts from C57BL/6 wild-type donors had a normal pseudostratified respiratory epithelium and no fibrotic occlusion (figure 1b). Confocal microscopy after immunofluorescent staining showed that >99% of all αSMA^+ cells in allograft lumens (defined as the area delineated by the inner edges of tracheal cartilages, which includes the submucosal space) were GFP^+, attesting their recipient origin (figure 1c, d). Of note, about half of these cells stained positive for CD45, a haematopoietic marker.

Tacrolimus treatment reduces post-transplant obliterative lesions and allows the survival of donor-derived myofibroblasts in the allografts

Although the above findings are in line with recent data [18], they seem to exclude donor cells as potential sources of fibrosis, and do not fit with the conclusions of some *ex vivo* studies [10, 11]. Therefore, as a means to reduce the gap between our experimental model and the clinical settings of BOS development, we treated recipient mice with tacrolimus (FK506), an immunosuppressant drug used in >80% of patients with lung transplants [2]. Previous pharmacokinetic studies in mice showed that an intraperitoneal dose of 1 $mg \cdot kg^{-1} \cdot day^{-1}$ of tacrolimus produced blood levels in the human therapeutic range [19]. Hence, C57BL/6

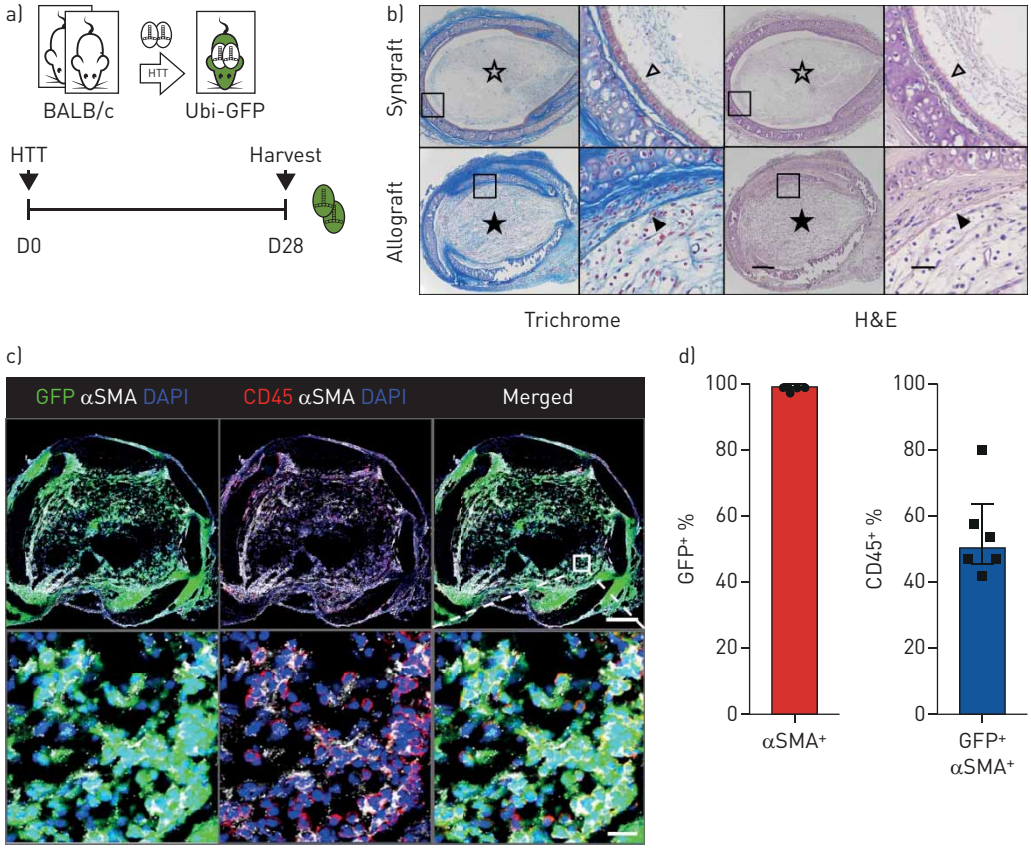

FIGURE 1 Almost all intragraft myofibroblasts derive from recipient cells at day 28 (D28) post-heterotopic tracheal transplantation (HTT). a) Experimental design: two BALB/c tracheas were subcutaneously engrafted into each Ubi-GFP (C57BL/6 background) recipient to obtain a complete allogeneic mismatch (allografts). C57BL/6 donors were used to obtain syngeneic controls (syngrafts). All grafts were harvested at D28. b) Representative images of Masson's trichrome and haematoxylin and eosin (H&E) staining of tracheal syngrafts (C57BL/6 donor) and allografts (BALB/c donor) at D28. Empty stars show mucus and cellular debris in the syngraft lumen, testifying to the normal epithelial function. Black stars show complete obliteration of the allograft lumens by fibrotic tissue. Empty arrowheads show a normal pseudostratified respiratory epithelium. Black arrowheads indicate the absence of epithelium on the lamina basalis. Scale bars: 200 and 40 µm. c) Representative confocal images of an allograft (BALB/c into Ubi-GFP mice) at D28 post-HTT, showing GFP, CD45, αSMA and DAPI co-stainings. Scale bars: 200 and 20 µm. d) Quantification of recipient-derived myofibroblasts (GFP^+ αSMA^+) and CD45 expression among recipient-derived myofibroblasts in fibrotic airways, based on confocal pictures (n=6 allografts). Data are presented as median±interquartile range.

Ubi-GFP recipients were treated daily with vehicle only (mock group) or 1 mg·kg^{-1} tacrolimus (T1 group) from day 0 to day 28 post-HTT (figure 2a). Tacrolimus whole-blood concentrations were measured using a liquid chromatography-mass spectrometry (LC-MS) assay at 3 h post-dose (C3) (figure 2b), and showed drug levels similar to those found in transplanted patients [20, 21]. After 28 days, histological quantification

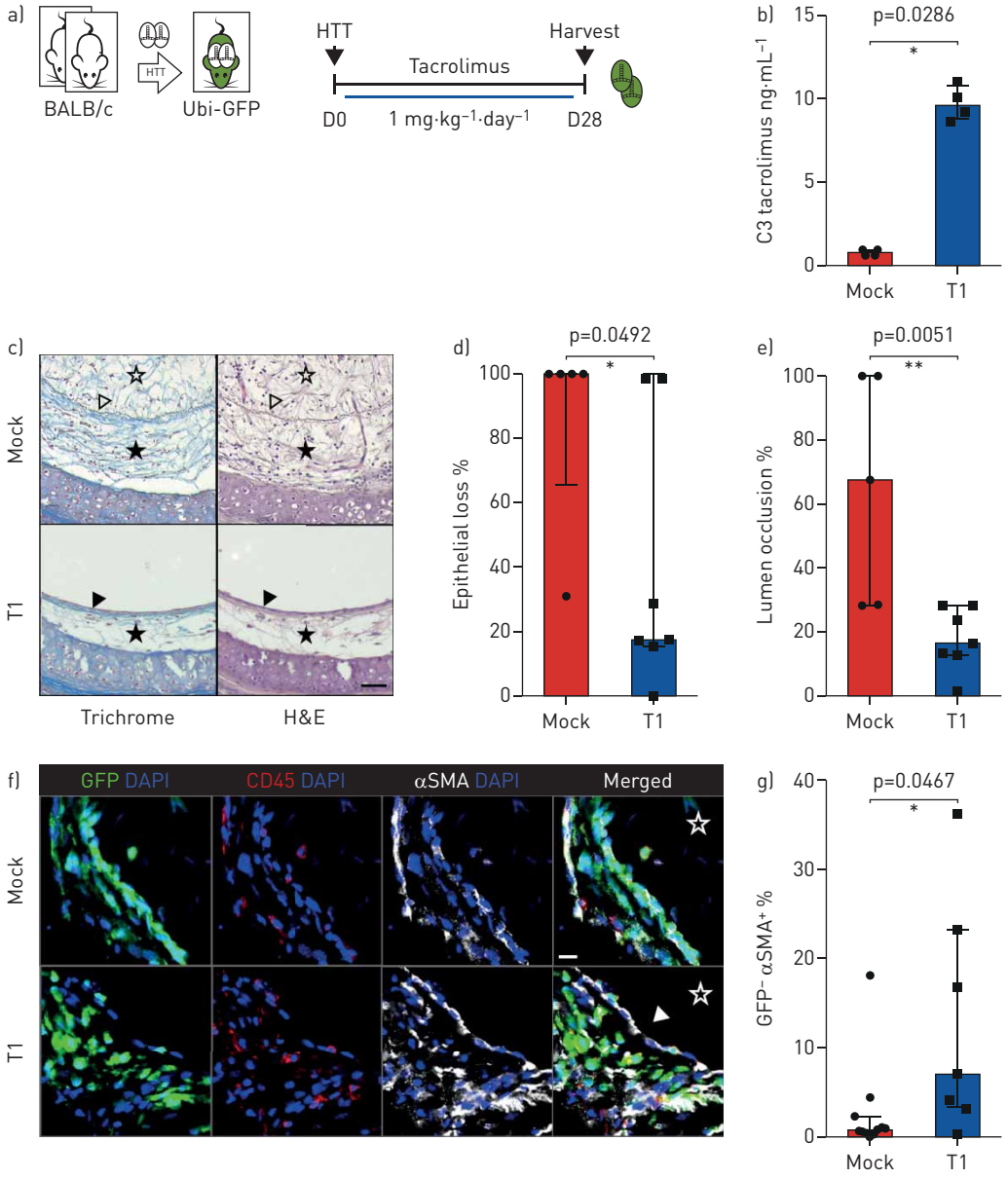

FIGURE 2 Tacrolimus inhibits obliterative airway disease development and increases the proportion of donor-derived myofibroblasts at day 28 (D28) post-heterotopic tracheal transplantation (HTT). a) Experimental design: two BALB/c tracheas were implanted into an Ubi-GFP recipient. Recipients received either 1 mg·kg^{-1} of tacrolimus (T1) or vehicle only (Mock) via intraperitoneal daily injections. All grafts were harvested at D28 post-HTT. b) Whole-blood levels of tacrolimus at 3 h post-dose (C3) measured by liquid chromatography-mass spectrometry (n=4 mice). c) Representative histological pictures of a mock-treated allograft compared to a tacrolimus-treated allograft at D28. Masson's trichrome and haematoxylin and eosin (H&E) staining. Empty stars show intraluminal fibrosis. Empty arrowheads indicate the lamina basalis. Black stars identify submucosal fibrosis. Black arrowheads show the flattened respiratory epithelium. Scale bar: 50 µm. d, e) Quantification of epithelial loss (d) and luminal occlusion (e) in the allografts (n=5–7 independent allografts). Data are presented as median±interquartile range. f) Representative confocal images of the allografts with or without tacrolimus treatment. Empty stars indicate the lumen. White arrowhead points to donor-derived myofibroblasts, which are negative for GFP and CD45 and positive for αSMA. Nuclei are stained with DAPI. Scale bar: 30 µm. g) Quantification of the proportion of donor-derived myofibroblasts (GFP$^-$ αSMA$^+$) based on confocal images. Each dot represents a BALB/c graft from an Ubi-GFP recipient at D28 post-HTT (n=7–11 per group). Data are presented as median±interquartile range. *: p<0.05; **: p<0.01.

of epithelial loss and lumen occlusion revealed a significant although heterogeneous effect of tacrolimus in reducing both parameters (figure 2c–e). Furthermore, under tacrolimus treatment, we were able to detect donor-derived GFP$^-$ cells among the luminal αSMA$^+$ population, although the proportion of these cells remained generally low (7%) (figure 2f, g). We therefore conclude that reducing the allogeneic reaction allows the survival of donor-derived mesenchymal cells that might contribute to luminal occlusion.

We next sought to test the existence of EMT phenomena under tacrolimus treatment. KRT5-Cre^{ERT2} knock-in mice on a mixed genetic background [22] were crossed with Rosa26-tdTomato reporter mice to obtain tdTomato expression in epithelial cells after tamoxifen induction (K5-TOM$^+$) (supplementary figure S1b). K5-TOM$^+$ tracheas were then transplanted into either C57BL/6 wild-type (allogeneic group) or CD3ε$^{-/-}$ recipients (used as the control non-rejected group because these mice lack T-lymphocytes) and harvested 7 days after HTT, when early lesions due to alloreactivity start to appear but the epithelial layer is preserved (supplementary figure S1a). About 20% of tdTomato$^+$ epithelial cells in the allografts expressed the mesenchymal marker αSMA (against only ∼3% in the non-rejected group) (supplementary figure S1c, d). Next, we transplanted K5-TOM$^+$ tracheas into Ubi-GFP mice that were treated or not with tacrolimus (supplementary figure S1e). At day 28 post-HTT, a small fraction of epithelial-derived (tdTomato$^+$) myofibroblasts (αSMA$^+$) (median 1.7%; up to 14% in two out of five samples) was detected exclusively in tacrolimus-treated allografts (p=0.007) (supplementary figure S1f, g). Donor-derived (GFP$^-$) αSMA$^+$ cells with no evident epithelial origin (tdTomato$^-$) accounted instead for <10% of all myofibroblasts in treated recipients. These data suggest that EMT processes might happen in allografts under circumstances of attenuated alloreactivity, but constitute only a fraction of all donor-derived mesenchymal cells.

Cells from the myeloid lineage give rise to the majority of myofibroblasts found in obliterative airways fibrosis

Even under tacrolimus treatment, recipient cells remained the main source for intragraft myofibroblasts in our OAD model (figure 2g), and a consistent proportion of recipient-derived αSMA$^+$ myofibroblasts co-expressed the haematopoietic marker CD45 (figure 1d). Accordingly, we decided to further assess the role of recipient haematopoietic progenitors by using VAV1-CRE;Rosa26-tdTomato (VAV1-TOM) mice as recipients (supplementary figure S2a, b) [7]. Of note, given the scarcity of recipient-derived cells infiltrating the syngeneic grafts from Ubi-GFP recipients at day 28 (supplementary figure S3), no further syngeneic HTTs were performed in the following lineage-tracing experiments. Fluorescence microscopy after nuclear (DAPI), mesenchymal (αSMA) and haematopoietic (CD45) immunostainings indicated that >90% of intragraft live myofibroblasts did indeed arise from tdTomato$^+$ haematopoietic cells (supplementary figure S2c, d).

We next explored the hypothesis that myeloid-derived fibrocytes represent a potential source of myofibroblasts [10, 23–25]. LysM-CRE;Rosa26-tdTomato recipients (LysM-TOM) were used to track myeloid cells in our HTT model (figure 3a), and the efficiency of the fate-mapping strategy was first confirmed by flow cytometry (figure 3b) [26]. Four-colour confocal analysis showed the co-localisation of αSMA, tdTomato and myeloid marker CD11b in the allograft lumens (figure 3c). Further quantification revealed that most αSMA$^+$ cells in obliterative lesions derived from LysM$^+$ cells, and also indicated that more than 20% of these myeloid-derived myofibroblasts expressed the macrophage marker F4/80 (figure 3d, e). Moreover, we noticed a positive correlation between the severity of luminal fibrosis and the proportion of myeloid-derived myofibroblasts in the allografts (figure 3f). These results demonstrate that recipient-derived myeloid precursors were the main source of myofibroblasts in rejected airways.

The MPS represents a potential source of myofibroblasts

To take a closer look at LysM-lineage mesenchymal progenitors, we isolated tdTomato$^+$ cells from LysM-TOM allografts by flow cytometry and subjected these cells to single-cell RNA sequencing (scRNA-seq). TdTomato$^+$ splenocytes obtained from a LysM-TOM non-transplanted mouse were used as controls (figure 4a).

After exclusion of contaminating lymphoid cells, we generated a two-dimensional representation of tdTomato$^+$ single cells using the Uniform Manifold Approximation and Projection (UMAP) technique [27], which revealed separation of cells into several populations (figure 4b, c). We detected large clusters of macrophages (characterised by upregulation of *Adgre1*, *Ctsb*, *H2-Aa*, *Cd68*, *Cx3cr1*), monocytes (*Lyz2*, *Ly6c2*, *Ccr2*, *S100a4*, *Vcan*), granulocytes (*Cxcr2*, *S100a8*, *S100a9*, *Csf3r, MMP9*) and fibrocytes (*Lum*, *Postn*, *Col1a2*, *Fn1*, *Ctgf*, *Cd34*, *Pdgfra*) (supplementary figure S4a). We observed clear differences between macrophages depending on their origin, such as higher expression of *Mafb*, *Mertk* and *Vim* in those from the allografts (figure 4c, d and supplementary figure S4b). Of note, increased expression of *Mertk* and *Mafb* in macrophages has previously been associated with idiopathic pulmonary fibrosis (IPF) [28, 29].

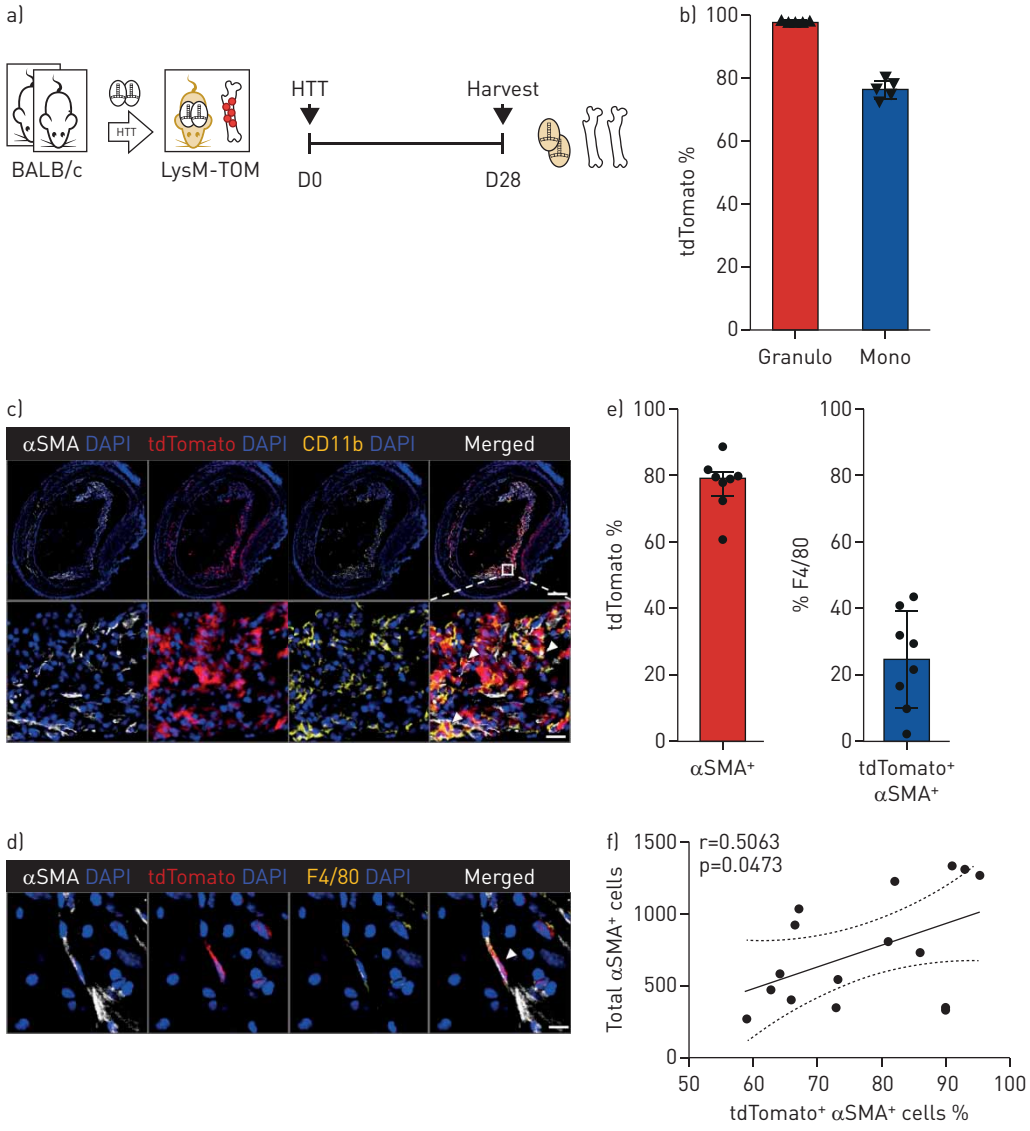

FIGURE 3 Recipient myeloid cells give rise to the majority of intragraft myofibroblasts. a) Experimental design: two BALB/c tracheas were engrafted into each LysM-TOM recipient. At day 28 (D28) post-heterotopic tracheal transplantation (HTT), all tracheal grafts and bone marrows were harvested and analysed by confocal microscopy or flow cytometry, respectively. b) Flow cytometry quantification of tdTomato expression in granulocytes (granulo) ($CD45^+$ LIN^- $CD11b^+$ $Ly6G^+$) and monocytes (mono) ($CD45^+$ LIN^- $Ly6G^-$ $CD11b^+$ $Ly6C^{hi}$) from LysM-TOM bone marrows (n=5 mice). c) Representative confocal pictures of a LysM-TOM allograft at D28 post-HTT. Arrowheads in the merged lower picture show several cells co-localising for αSMA (white), tdTomato (red) and CD11b (yellow) from a fibrotic area of the allograft lumen. Scale bars: 200 µm and 20 µm. d) Detail of a fibrotic allograft. Arrowhead in merged picture indicates an $αSMA^+$, $tdTomato^+$ and $F4/80^+$ cell in the lumen. Scale bar: 10 µm. e) Confocal microscopy quantification of tdTomato and F4/80 expression among $αSMA^+$ myofibroblasts or myeloid-derived $tdTomato^+$ $αSMA^+$ myofibroblasts (n=8 allografts). Data are presented as median±interquartile range. f) Positive correlation between the total number of $αSMA^+$ cells per section and the fraction of myeloid-derived myofibroblasts ($tdTomato^+$ $αSMA^+$) found in allograft lumens at D28 post-HTT. Each dot represents one allograft section analysed by confocal microscopy.

Few cells expressed *Acta2* (encoding αSMA), probably because sample processing and microfluidic encapsulation excluded fully differentiated myofibroblasts (see Methods), which in their activated form can reach up to 100 µm long [30, 31]. Despite this important limitation, we observed pronounced expression of *Pdgfrb* and *Col1a2* in fibrocytes and some allograft macrophages (macrophages 1) (figure 4d and supplementary figure S4a). The rare population of $tdTomato^+$ fibrocytes obtained from the allografts was markedly positive for a list of genes identified in human myofibroblasts from IPF patients (figure 4e) [33]. This population of myeloid-derived mesenchymal cells did not express markers of proliferation (supplementary figure S4d). The gene coding for lumican (*Lum*) was also highly upregulated in graft

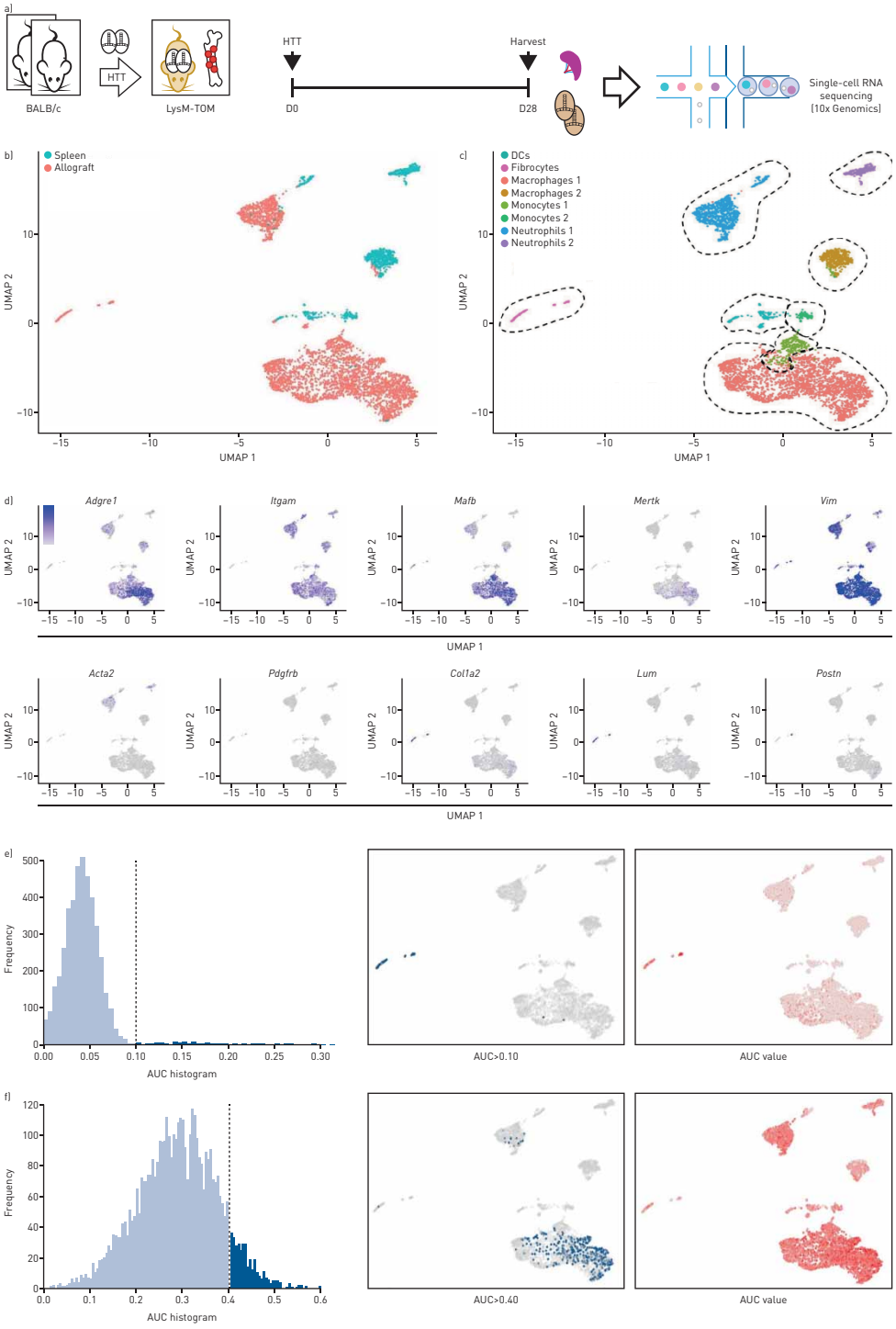

FIGURE 4 Single-cell RNA-sequencing analysis reveals pro-fibrotic macrophage and fibrocyte populations in the allografts. a) Experimental design: two BALB/c tracheas were transplanted into each LysM-TOM mouse and harvested at day 28 (D28). All tdTomato^{+} cells from 10 allografts and one LysM-TOM spleen underwent fluorescence-activated cell sorting and were analysed using 10x Genomics single-cell RNA sequencing. b, c) Uniform Manifold Approximation and Projection (UMAP) plots of spleen (green) and allografts (red) single cells segregated into eight different clusters according to their patterns of gene expression (c) (supplementary figure S4a). DC: dendritic cell. d) UMAP plots showing absolute expression (log-normalised count) of the indicated genes. Colour scale varies from 0 to 1.5 (*Mertk*), 2 (*Acta2*, *Pdgfrb*), 2.5 (*Itgam*), 3 (*Adgre1*, *Mafb*, *Lum*, *Postn*) or 5 (*Vim*, *Col1a2*). e, f) Area under the curve (AUC) distributions for specific gene sets (gene signatures) scored on each single cell from our data set using AUCell R package [32]. The histograms represent the AUC distribution of a gene set identified in e) human myofibroblasts from idiopathic pulmonary fibrosis patients [33] or f) pro-fibrotic macrophages found in bleomycin-treated lungs [29]. The UMAP plots on the left show the cells with AUC values passing the threshold in blue, while on the right the cells are coloured in shades of red according to the AUC value for each given gene set.

fibrocytes (figure 4d). Increased levels of this small proteoglycan have already been correlated with monocyte-to-fibrocyte differentiation *in vitro* and advanced disease in patients with lung fibrosis [25]. Periostin (*Postn*), a matricellular protein, was highly expressed in a group of fibrocytes (figure 4d and supplementary figure S4a). It has been suggested that periostin induces myofibroblast differentiation and lung fibrosis in a bleomycin model [34]. Moreover, the macrophages in the allografts (macrophages 1) were strongly enriched for the pro-fibrotic signature found in bleomycin-treated lungs (figure 4f) [28].

To further investigate the link between the MPS and airway fibrosis, we examined allografts from LysM-TOM recipients using flow cytometry and characterised myeloid-derived tdTomato$^+$ αSMA$^+$ cells (figure 5a). Among these cells, the majority expressed CD11b, up to 40% co-expressed F4/80 and CD64 (two classical macrophage markers) and smaller fractions expressed Ly6C (13.8%) and Ly6G (11.1%), markers for monocytes and granulocytes, respectively (figure 5b, c). In addition, Cx3cR1 and CD68 were highly expressed by those myeloid-derived αSMA$^+$ macrophages (supplementary figure S5b, d, e). These data, along with those obtained by confocal microscopy, support the notion that myeloid cells, and

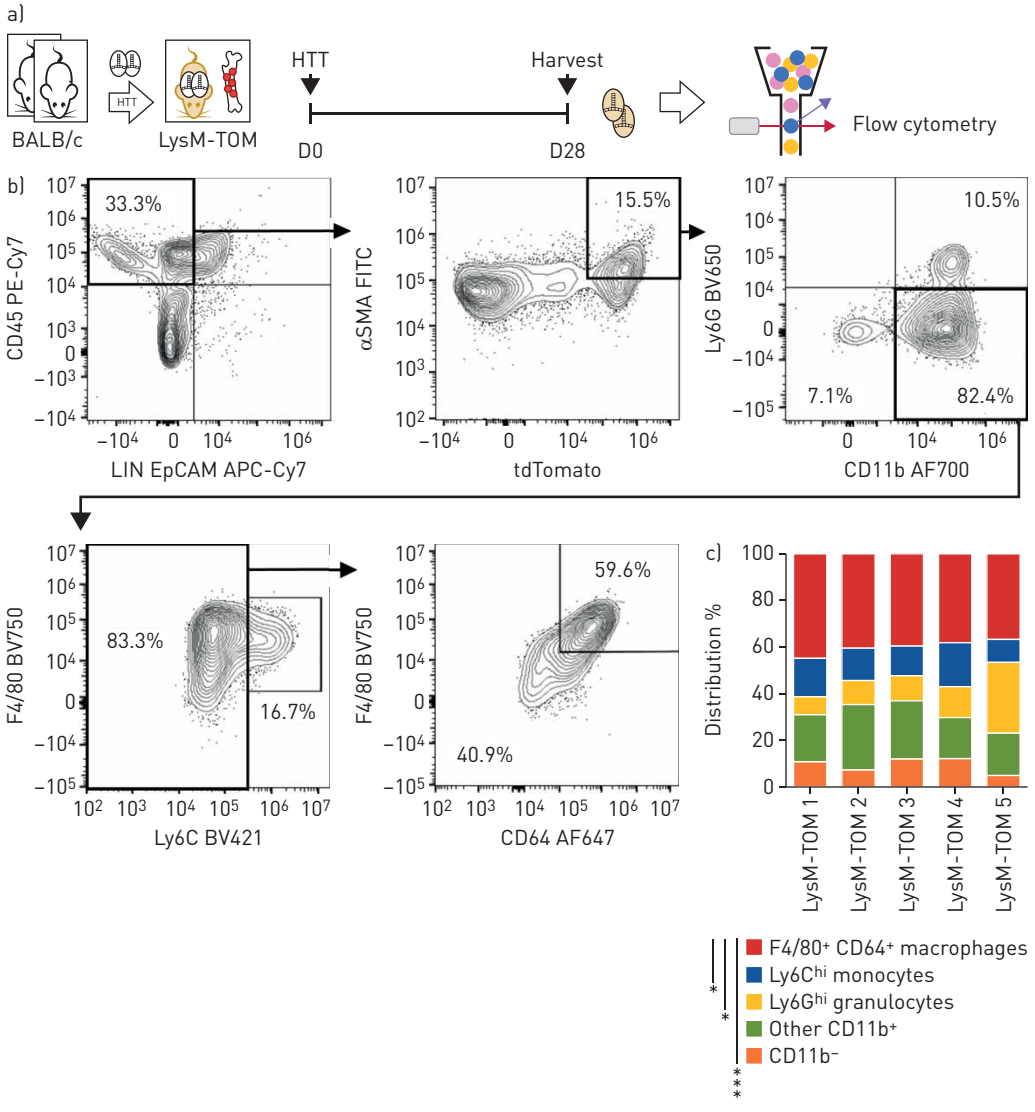

FIGURE 5 Phenotypic characterisation of myeloid-derived αSMA$^+$ cells. a) Experimental design: each LysM-TOM mouse received two BALB/c tracheas. 28 days (D28) after surgery, allografts from the same LysM-TOM recipient were pooled together and analysed by flow cytometry. b) Gating strategy for LysM-TOM-derived allografts. c) Relative distribution of macrophages (CD45$^+$ LIN$^-$ EpCAM$^-$ CD11b$^+$ Ly6G$^-$ Ly6C$^-$ F4/80$^+$ CD64$^+$), monocytes (CD45$^+$ LIN$^-$ EpCAM$^-$ CD11b$^+$ Ly6G$^-$ Ly6C^{hi}), granulocytes (CD45$^+$ LIN$^-$ EpCAM$^-$ CD11b$^+$ Ly6G$^+$) and other CD11b$^+$ or CD11b$^-$ populations among myeloid-derived (tdTomato$^+$) αSMA$^+$ cells from allografts at D28 post-heterotopic tracheal transplantation (HTT).

specifically the monocyte-macrophage population, could differentiate into activated myofibroblasts in a pro-fibrogenic environment.

Cx3cR1-lineage cells express mesenchymal marker αSMA and synthesise proCollagen I

Based on these results, we sought to evaluate the specific contribution of the MPS, using Cx3cR1-CRE^{ERT2}; Rosa26-tdTomato (Cx3cR1^{creER}-TOM) as recipients. tdTomato expression was induced by a tamoxifen-containing diet from day 0 until day 28 post-HTT, and confirmed by flow cytometric analysis on Cx3cR1^{creER}-TOM bone marrow, spleens and allografts (figure 6a–d). Compared to the LysM-CRE system, tdTomato expression was more specific for the mononuclear phagocyte lineage, because granulocytes were not as efficiently targeted. Additionally, only a minority of T-cells were tdTomato$^+$. Confocal acquisition of allografts showed that 40% of αSMA$^+$ cells co-localised for the fluorescent reporter tdTomato, and among these myeloid-derived myofibroblasts the majority were positive for CD45, while almost 30% expressed the macrophage marker F4/80 (figure 6e–g). To assess the participation of Cx3cR1-lineage cells in extracellular matrix deposition, all allografts were co-labelled for proCollagen1A1 (proCOL1A1), along with CD11b. Confocal analysis showed that most proCOL1A1$^+$ cells were tdTomato$^+$. Moreover, ∼40% of all proCOL1A1$^+$ cells maintained the expression of CD11b, and a similar proportion was observed among the tdTomato$^+$ proCOL1A1$^+$ population (figure 6h, i). Overall, these data support the implication of monocyte-derived collagen-producing mesenchymal cells in luminal fibrosis post-HTT.

Ablation of Cx3cR1$^+$ cells decreases fibrotic occlusion and myofibroblast accumulation in allografts

To further evaluate the role of the monocyte-macrophage lineage in the fibrotic process, we induced a diphtheria toxin A (DTA)-mediated, time-controlled deletion of Cx3cR1$^+$ cells in Cx3cR1-CRE^{ERT2}; Rosa26-DTA (Cx3cR1-DTA) recipients. A group of Cx3cR1-DTA mice received BALB/c trachea transplantations and were fed a tamoxifen diet (Cx3cR1-DTA^{tx}) (figure 7a). BALB/c tracheas harvested from tamoxifen-treated C57BL/6 wild-type recipients or Cx3cR1-DTA non-treated recipients were used as controls. DTA-mediated specific depletion of F4/80$^+$ macrophages was verified by flow cytometric analysis (figure 7b). Immunofluorescent staining demonstrated a significant reduction of F4/80$^+$ cells (p=0.007) but also a decrease of αSMA$^+$ myofibroblasts in the lumen of Cx3cR1-DTA^{tx} allografts (p=0.002) (figure 7c, d). Similarly, Masson's trichrome staining showed a reduction of lumen occlusion after Cx3cR1$^+$ cell ablation (p=0.0151), while there was no effect on epithelial rejection (figure 7e, f). Of note, ablation of Cx3cR1$^+$ cells did not affect the proportion of T-cells in the spleen nor their density in the allografts (figure 7b, g, h). Collectively, these data indicate that the MPS plays a central role in airway fibrosis after allogeneic transplantation.

CD68$^+$ myofibroblasts are detected in fibrotic lesions from human BOS explants

To translate our experimental findings we explored the potential role of myeloid-derived cells in human BOS fibrosis after lung transplantation. First, histological assessments confirmed the presence of typical OB lesions in the lungs from BOS patients [35], and the absence of fibrotic remodelling in control lungs (figure 8a). Immunofluorescent staining revealed several CD45$^+$ αSMA$^+$ myofibroblasts in the fibro-obliterated bronchioles of rejected lungs (figure 8b). Hence, we co-stained the lungs for αSMA and CD68, a classical marker for murine (supplementary figure S5) and human (figure 8c) macrophages. As expected, confocal quantifications showed a general increase of αSMA$^+$ cells in BOS sections (figure 8d). Importantly, we observed a significant accumulation of CD68$^+$ myofibroblasts when compared to healthy controls (14.4% *versus* 8.5% of all αSMA$^+$ cells, p=0.0249) (figure 8e, f). Finally, the fraction of CD68$^+$ myofibroblasts was directly related to the total number of myofibroblasts found in each lung section, suggesting that the severity of the fibrosis correlates with the presence of myeloid-derived αSMA$^+$ mesenchymal cells (figure 8g, h). Altogether, these clinical results are consistent with our experimental findings, and imply the involvement of MPS-derived myofibroblasts in human BOS development.

Discussion

The identification of mesenchymal cell origins is a critical goal in studies on fibrotic diseases such as BOS. Here, we demonstrate that the majority of myofibroblasts present in rejected allogeneic tracheas are recipient-derived. Our results are similar to those obtained by Konoeda *et al.* [15], where the lower contribution of recipient cells (∼75%) could be explained by several differences in experimental settings. Despite the limitations of the HTT model [36], our findings are in line with those obtained by Sato *et al.* [37], who used an *in vivo* model to demonstrate that almost all myofibroblasts were of extrapulmonary origin. We further show that most of these mesenchymal cells arise from myeloid precursors. Despite a large degree of heterogeneity, an important proportion of mesenchymal cells expressed typical macrophage markers.

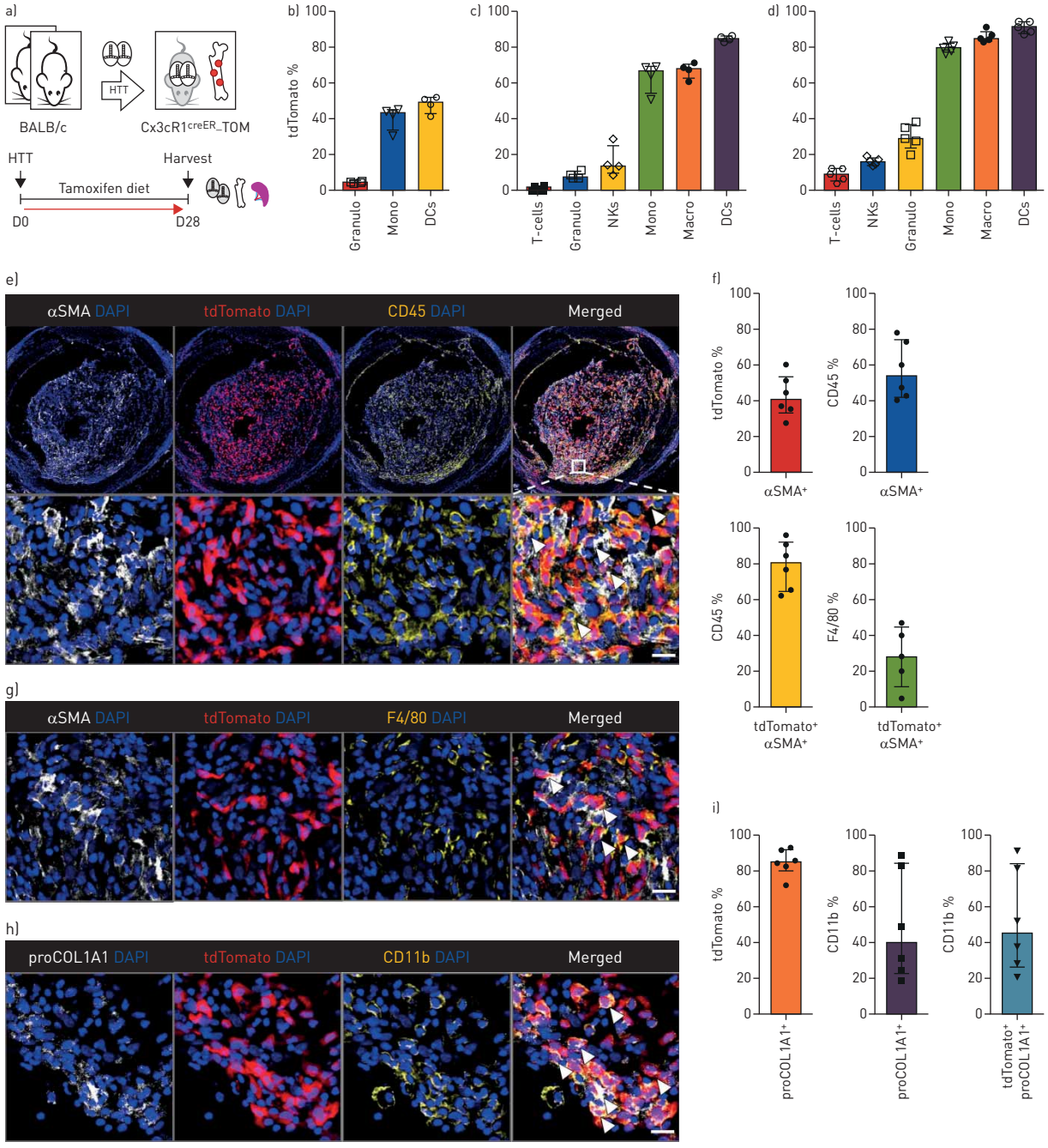

FIGURE 6 The mononuclear phagocyte system contributes to the myofibroblast population and participates in proCollagen I production. a) Experimental design used to track the Cx3cR1^{+} lineage during allograft rejection: two BALB/c tracheas were transplanted heterotopically on each Cx3cR1^{creER}-TOM recipient. The expression of the fluorescent reporter tdTomato was induced by feeding the recipients with a tamoxifen-containing diet from day 0 until day 28 (D28) post-heterotopic tracheal transplantation (HTT). At D28, all tracheal grafts and recipient bone marrow and spleens were harvested and analysed by flow cytometry or confocal microscopy. b–d) Flow cytometry analysis of Cx3cR1^{creER}-TOM b) bone marrows (n=4), c) spleens (n=4) and d) allografts (n=5 samples, each dot representing two pooled allografts from the same recipient) showing tdTomato expression in granulocytes (granulo) (CD45^{+} LIN^{-} CD11c^{-} CD11b^{+} Ly6G^{+}), monocytes (mono) (CD45^{+} LIN^{-} CD11c^{-} Ly6G^{-} CD11b^{+} Ly6C^{hi}), macrophages (macro) (CD45^{+} LIN^{-} CD11c^{-} Ly6G^{-} CD11b^{+} Ly6C^{-} F4/80^{+}), dendritic cells (DCs) (CD45^{+} LIN^{-} CD11c^{hi}), natural killer cells (NKs) (CD45^{+} CD3ε^{-} CD19^{-} NK1.1^{+}) and T-cells (CD45^{+} CD3ε^{+} CD19^{-} in spleens and CD45^{+} CD3ε^{+} NK1.1^{-} in allografts) after 4 weeks of tamoxifen diet induction. e) Representative confocal picture of a BALB/c allograft from a Cx3cR1^{creER}-TOM recipient at D28 post-HTT. A detail from the graft lumen is displayed in the lower merged picture, where several cells co-localise for αSMA, tdTomato and CD45 as indicated by arrowheads. Scale bars: 200 µm and 20 µm. f) Confocal microscopy quantification of tdTomato, CD45 and F4/80 expression among αSMA^{+} myofibroblasts or myeloid-derived tdTomato^{+} αSMA^{+} myofibroblasts (n=6 allografts). g) Representative confocal picture of the lumen of an allograft from a Cx3cR1^{creER}-TOM recipient, where the arrowheads indicate the co-localisation of αSMA, tdTomato and F4/80 in the same cell. Sale bar: 20 µm. h) Representative confocal picture of a Cx3cR1^{creER}-TOM-derived allograft. Several cells in the luminal fibrosis (merged figure, arrowheads) are positive for proCollagen1a1 (proCOL1A1), tdTomato and CD11b. Scale bar: 20 µm. i) Quantification based on confocal analysis of tdTomato and CD11b expression among proCOL1A1^{+} cells or myeloid-derived (tdTomato^{+}) proCOL1A1^{+} cells found in the lumen of allografts at D28. Each dot represents one allograft (n=6 samples). Data are presented as median±interquartile range.

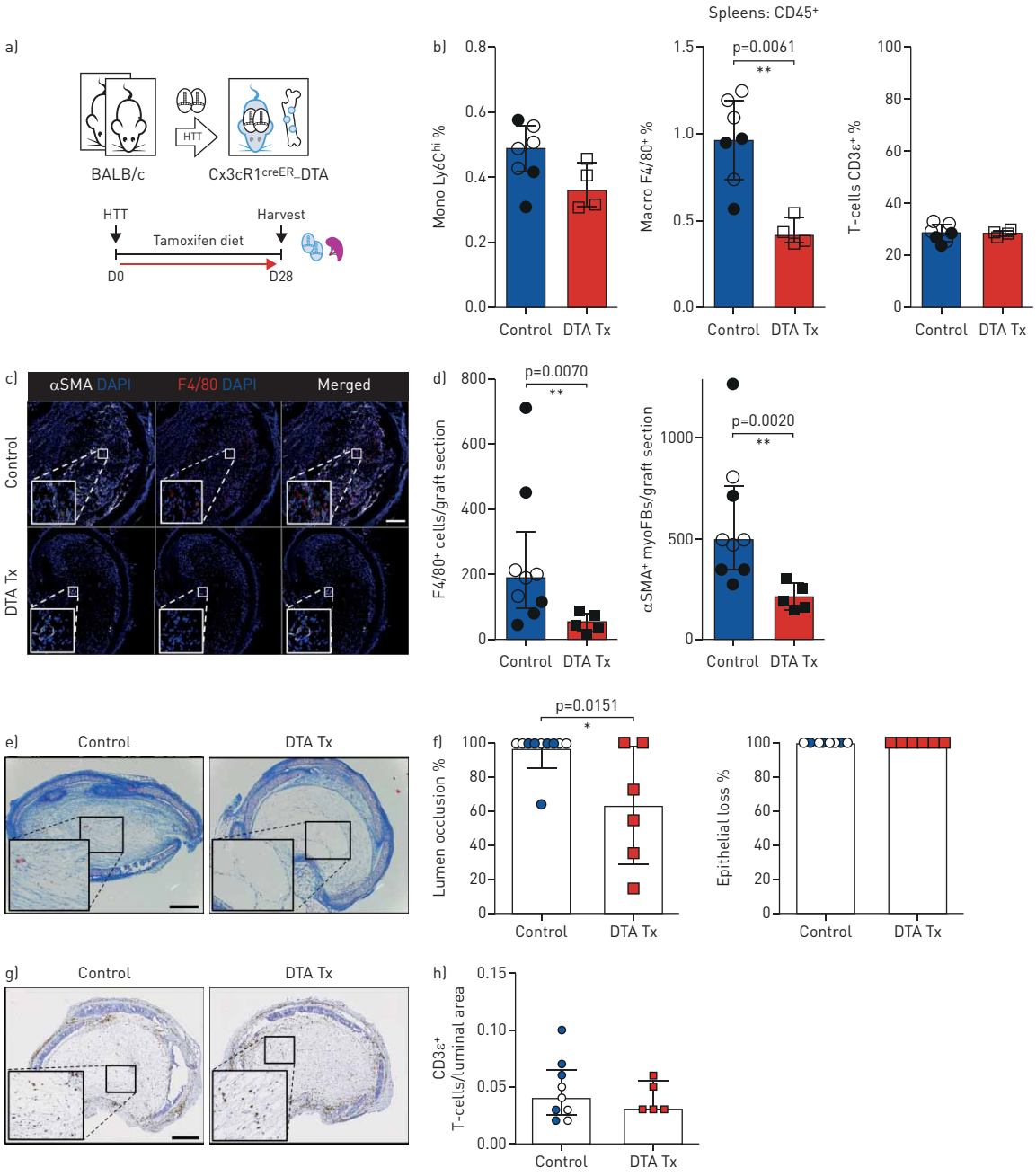

FIGURE 7 Selective depletion of Cx3cR1-expressing cells is associated with reduced occlusion and decreased myofibroblast (myoFB) accumulation in allograft lumens. a) Experimental design: two BALB/c tracheas were transplanted into each Cx3cR1^{creER}-DTA recipient. The treated group (DTA Tx) was fed with a tamoxifen-containing diet to induce diphtheria toxin A (DTA) cytosolic expression and consequent selective depletion of Cx3cR1^{+} cells. Cx3cR1^{creER}-DTA mice without tamoxifen induction and C57BL/6 wild-type mice fed with a tamoxifen diet were used as recipients in the control group. At day 28 (D28), all recipient spleens and allografts were analysed by flow cytometry, or histology and confocal microscopy, respectively. b) The proportion of monocytes (CD3ε^{-} CD19^{-} CD11c^{-} Ly6G^{-} CD11b^{+} Ly6C^{hi}), macrophages (CD3ε^{-} CD19^{-} CD11c^{-} Ly6G^{-} CD11b^{+} F4/80^{+} Ly6C^{-}) and T-cells (CD3ε^{+} CD19^{-}) among CD45^{+} splenocytes assessed by flow cytometry analysis (each point represents an individual mouse, n=4–7 per group). Among the controls, black circles represent Cx3cR1^{creER}-DTA mice without tamoxifen induction, whereas empty circles correspond to C57BL/6 wild-type mice fed with tamoxifen diet. c) Representative confocal pictures of a control allograft (Cx3cR1^{creER}-DTA recipient without tamoxifen induction) compared to an allograft from a Cx3cR1^{creER}-DTA tamoxifen-treated recipient (DTA Tx) at D28 post-surgery. Scale bar: 200 µm. d) Confocal quantification of F4/80^{+} and αSMA^{+} cells found in the allograft lumens as shown in c. The black circles represent the allografts from Cx3cR1^{creER}-DTA recipients without tamoxifen induction, whereas the empty circles correspond to allografts from C57BL/6 wild-type recipients treated with tamoxifen. e) Representative pictures of Masson's trichrome stained allografts at D28 post-transplant. A detail of the lumen at higher magnification is shown in the left corners; scale bar: 200 µm. f) Histological quantification of lumen occlusion and epithelial loss for each group of allografts (n=6–10 allografts). g) Immunohistochemical staining of CD3ε^{+} T-cells in allografts at D28 post-heterotopic tracheal transplantation (HTT); scale bar: 250 µm; h) histological quantification of CD3ε^{+} T-cells in the lumen of allografts with DTA-mediated Cx3cR1^{+} cells depletion *versus* controls. e–h) The empty circles correspond to the allografts from Cx3cR1^{creER}-DTA recipients without tamoxifen treatment, whereas the allografts from C57BL/6 tamoxifen-treated recipients are shown as blue circles in the control group. Data are presented as median±interquartile range. *: p<0.05; **: p<0.01.

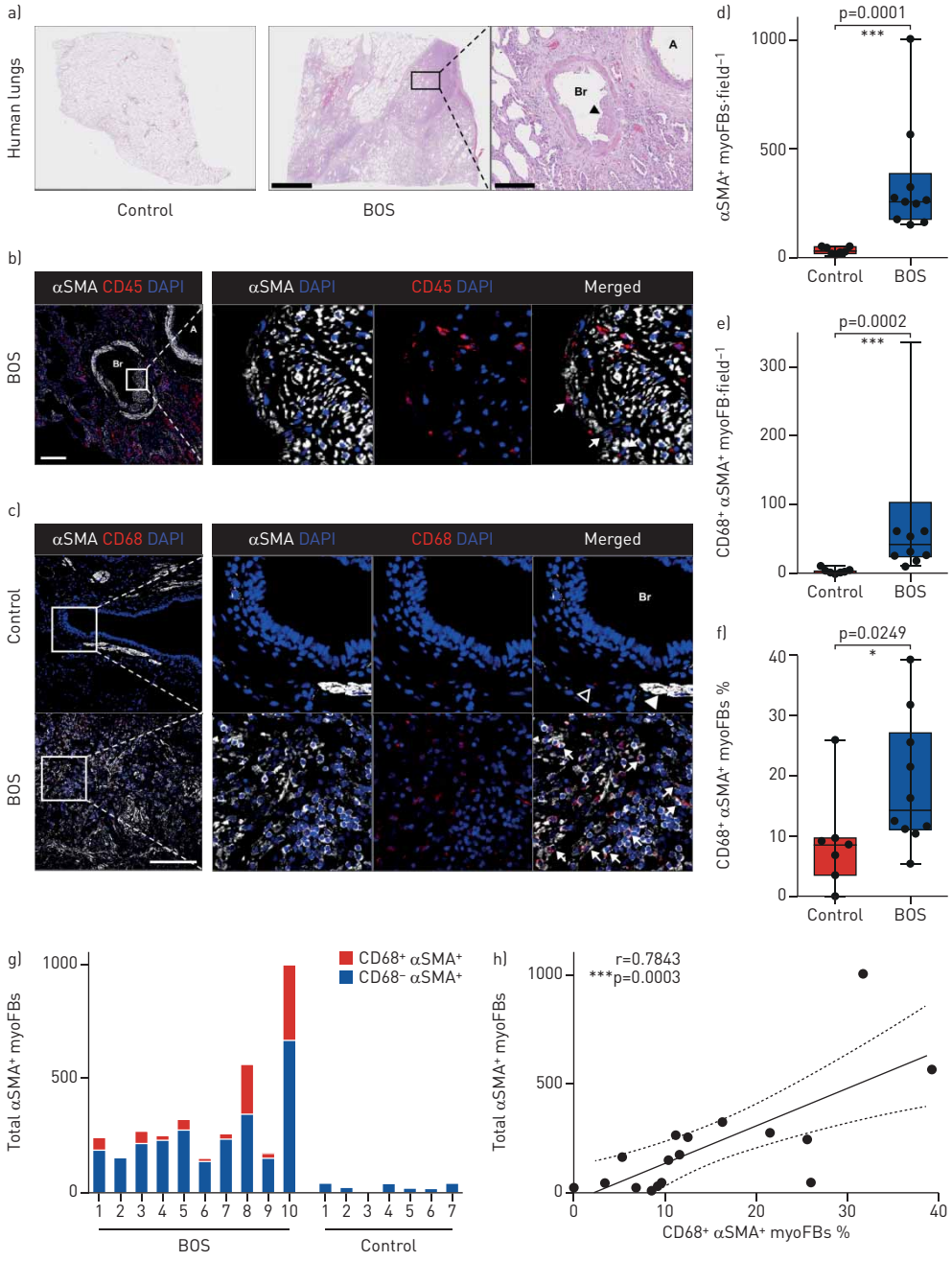

FIGURE 8 CD68$^+$ myofibroblasts (myoFB) are found in human bronchiolitis obliterans syndrome (BOS) explants. a) Representative scans of lung sections from control patients or patients with BOS. The higher magnification picture shows a bronchiole (Br) with typical obliterans bronchiolitis (OB) lesions, next to a small pulmonary artery (A). The black arrowhead in the bronchiole lumen indicates a polypoid plaque of dense scar tissue and the absence of epithelial layer. Haematoxylin and eosin staining. Scale bars: 5 mm and 250 µm. b) Representative confocal pictures showing OB lesions in the explanted lung from a BOS patient. In the merged picture, the white arrows indicate cells co-staining for αSMA and CD45 in the fibrotic lesion. Scale bar: 200 µm. c) Representative confocal pictures of healthy human lung tissue and a BOS explant co-stained for αSMA and CD68. White arrowhead indicates αSMA$^+$ smooth muscle cells. Empty arrowhead indicates CD68$^+$ cell. White arrows indicate αSMA$^+$ CD68$^+$ myoFBs in the BOS explant. Scale bar: 200 µm. d–f) Confocal analysis quantification for d) the total number of αSMA$^+$ myoFBs, e) αSMA$^+$ CD68$^+$ myoFBs and f) the fraction of αSMA$^+$ cells that co-localise for CD68, in healthy lungs *versus* BOS explant. All αSMA$^+$ smooth muscle cells were excluded from the count. Each dot represents the mean of four random fields (×200) quantified for each sample (n=7–10 patients per group). The central bar represents the median. g) Confocal quantification of the fraction of αSMA$^+$ cells co-localising for CD68 (red part of column) in each explant (BOS) or control sample. Four random fields (×200) were analysed for each sample (mean shown). h) Positive correlation between the total number of αSMA$^+$ myoFBs and the fraction of CD68$^+$ myoFBs found in human lungs (BOS and controls). Each dot represents the mean of four random fields from the same sample (n=17 patients). *: p<0.05; ***: p<0.001.

A previous study reported that recipient-derived cells represented one third of all αSMA$^+$ myofibroblasts in OB lesions [10]. However, the authors excluded all CD45$^+$ and CD68$^+$ cells during immunohistochemical assessments, therefore losing potential recipient-derived myofibroblasts of myeloid origin. Myeloid-derived mesenchymal cells found in the allografts showed very low rates of proliferation markers, confirming previous results [37]. Therefore, migration of precursors might represent the main mechanism for the accumulation of myofibroblasts and extracellular matrix deposition. Once monocytes migrate into the airways, differentiation into macrophages can be accompanied by the acquisition of mesenchymal features. In line with our hypothesis, Ishida *et al.* [38] revealed that the chemokine fractalkine promotes bleomycin-induced fibrosis by attracting Cx3cR1$^+$ macrophages and fibrocytes to the lung. Accordingly, an increasing number of studies suggest a major role of the MPS in chronic allograft diseases [39] and pulmonary fibrosis [28, 38, 40]. Recently, a subset of pathological Cx3cR1$^+$ macrophages was identified by single-cell analysis in bleomycin-induced lung fibrosis [28]. The same pro-fibrotic signature was highly activated in macrophages infiltrating the obliterated allografts in our model. With decreased airway luminal fibrosis upon Cx3cR1$^+$-cell depletion, our results confirm the implication of the MPS in OAD. Furthermore, we have demonstrated the presence of αSMA$^+$ myofibroblasts co-expressing the macrophage marker CD68 in human post-transplant OB lesions, thus reinforcing the potential implication of mononuclear phagocytes in clinical OB.

Our scRNA-seq analysis revealed the existence of a discrete population of myeloid-derived cells that express both haematopoietic and mesenchymal markers, and could represent an intermediate state between mononuclear phagocytes and αSMA^{high} myofibroblasts. Generally referred to as fibrocytes, these cells can differentiate into fibroblasts and myofibroblasts after entering the tissues [41]. This process can be associated with a loss of haematopoietic markers, such as CD45 and CD11b, making it more difficult to identify these cells with conventional techniques [7]. ScRNA-seq analysis revealed surprising similarities between mesenchymal cells from human IPF samples and fibrocytes in our BOS model [33]. High levels of lumican and periostin, implicated in monocyte-to-fibrocyte differentiation and myofibroblast activation during lung fibrosis, were also detected in allograft fibrocytes [25, 34]. Furthermore, *ex vivo* studies have identified a positive correlation between numbers of fibrocytes and development of BOS in patients with lung transplants, supporting the involvement of these myeloid-derived cells in OB pathogenesis [42, 43].

In a model of kidney fibrosis, LeBleu *et al.* [5] identified resident fibroblasts and non-proliferating bone marrow progenitors as the main sources of myofibroblasts, whereas epithelial cells only accounted for a minor fraction (5%). Consistent with this notion, we observed an increase in donor-derived myofibroblasts and identified rare epithelial-derived αSMA$^+$ cells in tacrolimus-treated allografts, a phenomenon that might be quite relevant to the clinical situation. Indeed, tacrolimus might 1) allow the survival of donor mesenchymal progenitors such as resident fibroblasts, 2) indirectly reduce migration of monocytes and macrophages to the graft [39], and 3) promote EMT phenomena in respiratory epithelial cells *via* aberrant transforming growth factor-ß signalling [13, 44, 45].

In summary, our data support the involvement of cells from the MPS in human BOS development after lung transplantation. Hence, the development of specific drug delivery systems that exploit the phagocytic properties of monocytes, macrophages and myofibroblasts [30] could lead to less toxic and more efficient anti-fibrotic treatments for BOS [39].

Acknowledgements: We are grateful to Laurence Vilain, Séverine Thomas and Muriel Nguyen (Institute for Medical Immunology, ULB, Gosselies, Belgium) and to Justine Allard and Egor Zindy (CMMI-Diapath, Gosselies, Belgium; supported by the European Regional Development Fund and the Walloon Region) for their invaluable help. We are thankful to Benjamin Beck (IRIBHM, ULB, Brussels, Belgium) and Christiane Knoop (Erasme Hospital, ULB, Brussels, Belgium) for insightful discussions, and to Frédéric Cotton (Erasme Hospital, ULB) for whole-blood tacrolimus assessments.

Author contributions: M-P. Di Campli performed most of the experiments and analysis. J. Scaillet, A. Assabban and A. Azouz contributed to some experiments. A. Azouz and M. Splittgerber performed bioinformatics analysis. M. Remmelink and A. Van Keymeulen helped with the interpretation of data and the conception of experiments. F. Libert performed next-generation sequencing sample processing and preliminary analysis. M-P. Di Campli, P. Lemaitre, A. Le Moine and S. Goriely conceived and designed the study. S. Goriely supervised the whole project. M-P. Di Campli and S. Goriely wrote the manuscript. All authors approved the final manuscript before submission.

Conflict of interest: None declared.

Support statement: This study was supported by the Fonds National de la Recherche Scientifique (FRS-FNRS, Belgium), the European Regional Development Fund (ERDF) of the Walloon Region (Wallonia-Biomed portfolio, 411132-957270), the Fonds pour la Chirurgie Cardiaque and the Fonds ERASME. S. Goriely is a senior research associate of the FRS-FNRS. M-P. Di Campli is supported by a FRIA-FNRS grant. Funding information for this article has been deposited with the Crossref Funder Registry.

References

1 Chambers DC, Cherikh WS, Goldfarb SB, *et al.* The International Thoracic Organ Transplant Registry of the International Society for Heart and Lung Transplantation: thirty-fifth adult lung and heart-lung transplant report—2018; focus theme: multiorgan transplantation. *J Heart Lung Transplant* 2018; 37: 1169–1183.
2 Chambers DC, Yusen RD, Cherikh WS, *et al.* The Registry of the International Society for Heart and Lung Transplantation: thirty-fourth adult lung and heart-lung transplantation report—2017; focus theme: allograft ischemic time. *J Heart Lung Transplant* 2017; 36: 1047–1059.
3 Verleden SE, Sacreas A, Vos R, *et al.* Advances in understanding bronchiolitis obliterans after lung transplantation. *Chest* 2016; 150: 219–225.
4 Agha E E, Kramann R, Schneider RK, *et al.* Mesenchymal stem cells in fibrotic disease. *Cell Stem Cell* 2017; 21: 166–177.
5 LeBleu VS, Taduri G, Teng Y, *et al.* Origin and function of myofibroblasts in kidney fibrosis. *Nat Med* 2013; 19: 1047–1053.
6 van Amerongen M, Bou-Gharios G, Popa E, *et al.* Bone marrow-derived myofibroblasts contribute functionally to scar formation after myocardial infarction. *J Pathol* 2014; 214: 199–210.
7 Suga H, Rennert RC, Rodrigues M, *et al.* Tracking the elusive fibrocyte: identification and characterization of collagen producing hematopoietic lineage cells during murine wound healing. *Stem Cells* 2014; 32: 1347–1360.
8 Xie T, Liang J, Liu N, *et al.* Transcription factor TBX4 regulates myofibroblast accumulation and lung fibrosis. *J Clin Invest* 2016; 126: 3063–3079.
9 Guilliams M, Ginhoux F, Jakubzick C, *et al.* Dendritic cells, monocytes and macrophages: a unified nomenclature based on ontogeny. *Nat Rev Immunol* 2014; 14: 571–578.
10 Bröcker V, Länger F, Fellous TG, *et al.* Fibroblasts of recipient origin contribute to bronchiolitis obliterans in human lung transplants. *Am J Respir Crit Care Med* 2006; 173: 1276–1282.
11 Yousem SA, Sherer C, Fuhrer K, *et al.* Myofibroblasts of recipient origin are not the predominant mesenchymal cell in bronchiolitis obliterans in lung allografts. *J Heart Lung Transplant* 2013; 32: 266–268.
12 Hodge S, Holmes M, Banerjee B, *et al.* Posttransplant bronchiolitis obliterans syndrome is associated with bronchial epithelial to mesenchymal transition. *Am J Transplant* 2009; 9: 727–733.
13 Borthwick LA, Parker SM, Brougham KA, *et al.* Epithelial to mesenchymal transition (EMT) and airway remodelling after human lung transplantation. *Thorax* 2009; 64: 770–777.
14 Konoeda C, Koinuma D, Morishita Y, *et al.* Epithelial to mesenchymal transition in murine tracheal allotransplantation: an immunohistochemical observation. *Transpl Proc* 2013; 100: 130–134.
15 Konoeda C, Nakajima J, Murakawa T. Fibroblasts of recipient origin contribute to airway fibrosis in murine tracheal transplantations. *Transpl Int* 2015; 28: 761–763.
16 Hertz MI, Jessurun J, King MB, *et al.* Reproduction of the obliterative bronchiolitis lesion after heterotopic transplantation of mouse airways. *Am J Pathol* 1993; 142: 1945–1951.
17 Lemaître PH, Vokaer B, Charbonnier L, *et al.* Cyclosporine A drives a Th17- and Th2-mediated posttransplant obliterative airway disease. *Am J Transplant* 2013; 1: 611–620.
18 Watanabe S, Kasahara K, Waseda Y, *et al.* Imatinib ameliorates bronchiolitis obliterans via inhibition of fibrocyte migration and differentiation. *J Heart Lung Transplant* 2017; 36: 138–147.
19 Herbst S, Shah A, Carby M, *et al.* A new and clinically relevant murine model of solid-organ transplant aspergillosis. *Dis Model Mech* 2013; 6: 643–651.
20 Kim JH, Han N, Kim MG, *et al.* Model based development of tacrolimus dosing algorithm considering CYP3A5 genotypes and mycophenolate mofetil drug interaction in stable kidney transplant recipients. *Sci Rep* 2019; 9: 1–9.
21 Alloway RR, Vinks AA, Fukuda T, *et al.* Bioequivalence between innovator and generic tacrolimus in liver and kidney transplant recipients: a randomized, crossover clinical trial. *PLoS Med* 2017; 14: 1–22.
22 Van Keymeulen A, Rocha AS, Ousset M, *et al.* Distinct stem cells contribute to mammary gland development and maintenance. *Nature* 2011; 479: 189–193.
23 Reilkoff RA, Bucala R, Herzog EL. Fibrocytes: emerging effector cells in chronic inflammation. *Nat Rev Immunol* 2011; 11: 427–435.
24 Andersson-Sjöland A, de Alba CG, Nihlberg K, *et al.* Fibrocytes are a potential source of lung fibroblasts in idiopathic pulmonary fibrosis. *Int J Biochem Cell Biol* 2008; 40: 2129–2140.
25 Pilling D, Vakil V, Cox N, *et al.* TNF-α-stimulated fibroblasts secrete lumican to promote fibrocyte differentiation. *Proc Natl Acad Sci USA* 2015; 112: 11929–11934.
26 Meng XM, Wang S, Huang XR, *et al.* Inflammatory macrophages can transdifferentiate into myofibroblasts during renal fibrosis. *Cell Death Dis* 2016; 7: e2495.
27 Becht E, McInnes L, Healy J, *et al.* Dimensionality reduction for visualizing single-cell data using UMAP. *Nat Biotechnol* 2019; 37: 38–47.
28 Aran D, Looney AP, Liu L, *et al.* Reference-based analysis of lung single-cell sequencing reveals a transitional profibrotic macrophage. *Nat Immunol* 2019; 20: 163–172.
29 Morse C, Tabib T, Sembrat J, *et al.* Proliferating SPP1/MERTK-expressing macrophages in idiopathic pulmonary fibrosis. *Eur Respir J* 2019; 54: 1802441.
30 Nakaya M, Watari K, Tajima M, *et al.* Cardiac myofibroblast engulfment of dead cells facilitates recovery after myocardial infarction. *J Clin Invest* 2017; 127: 383–401.
31 Wang S, Meng X-M, Ng Y-Y, *et al.* TGF-β/Smad3 signalling regulates the transition of bone marrow-derived macrophages into myofibroblasts during tissue fibrosis. *Oncotarget* 2015; 7: 8809–8822.
32 Aibar S, González-Blas CB, Moerman T, *et al.* SCENIC: single-cell regulatory network inference and clustering. *Nat Methods* 2017; 14: 1083–1086.
33 Parker MW, Rossi D, Peterson M, *et al.* Fibrotic extracellular matrix activates a profibrotic positive feedback loop. *J Clin Invest* 2014; 124: 1622–1635.
34 Ashley SL, Wilke CA, Kim KK, *et al.* Periostin regulates fibrocyte function to promote myofibroblast differentiation and lung fibrosis. *Mucosal Immunol* 2016; 10: 1–11.
35 Stewart S, Fishbein MC, Snell GI, *et al.* Revision of the 1996 working formulation for the standardization of nomenclature in the diagnosis of lung rejection. *J Heart Lung Transplant* 2007; 26: 1229–1242.

36 Lama VN, Belperio JA, Christie JD, *et al.* Models of lung transplant research: a consensus statement from the National Heart, Lung, and Blood Institute workshop. *JCI Insight* 2017; 2: 1–14.
37 Sato M, Hirayama S, Lara-Guerra H, *et al.* MMP-dependent migration of extrapulmonary myofibroblast progenitors contributing to posttransplant airway fibrosis in the lung. *Am J Transplant* 2009; 9: 1027–1036.
38 Ishida Y, Kimura A, Nosaka M, *et al.* Essential involvement of the CX3CL1-CX3CR1 axis in bleomycin-induced pulmonary fibrosis via regulation of fibrocyte and M2 macrophage migration. *Sci Rep* 2017; 7: 16833.
39 van den Bosch TPP, Kannegieter NM, Hesselink DA, *et al.* Targeting the monocyte-macrophage lineage in solid organ transplantation. *Front Immunol* 2017; 8: 153.
40 Zhou X, Moore BB. Location or origin? What is critical for macrophage propagation of lung fibrosis? *Eur Respir J* 2018; 51: 1800103.
41 Florez-Sampedro L, Song S, Melgert BN. The diversity of myeloid immune cells shaping wound repair and fibrosis in the lung. *Regeneration* 2017; 5: 3–25.
42 LaPar DJ, Burdick MD, Emaminia A, *et al.* Circulating fibrocytes correlate with bronchiolitis obliterans syndrome development following lung transplantation: a novel clinical biomarker. *Ann Thorac Surg* 2012; 23: 1–7.
43 Andersson-Sjöland A, Erjefält JS, Bjermer L, *et al.* Fibrocytes are associated with vascular and parenchymal remodelling in patients with obliterative bronchiolitis. *Respir Res* 2009; 10: 1–11.
44 McMorrow T, Gaffney MM, Slattery C, *et al.* Cyclosporine A induced epithelial-mesenchymal transition in human renal proximal tubular epithelial cells. *Nephrol Dial Transplant* 2005; 20: 2215–2225.
45 Kern G, Mair SM, Noppert SJ, Jennings P, Schramek H, Rudnicki M, *et al.* Tacrolimus increases Nox4 expression in human renal fibroblasts and induces fibrosis-related genes by aberrant TGF-β receptor signalling. *PLoS One* 2014; 9: e96377.